HHS Public Access

Author manuscript

Calcif Tissue Int. Author manuscript; available in PMC 2023 February 01.

Published in final edited form as:

Calcif Tissue Int. 2022 February ; 110(2): 244–259. doi:10.1007/s00223-021-00903-7.

Nmp4, a Regulator of Induced Osteoanabolism, Also Influences Insulin Secretion and Sensitivity

Joseph Bidwell[1,2], **Sarah A. Tersey**[3,†], **Michele Adaway**[1], **Robert N. Bone**[3,6], **Amy Creecy**[4], **Angela Klunk**[1], **Emily G. Atkinson**[1], **Ronald C. Wek**[5], **Alexander G. Robling**[1,2], **Joseph M. Wallace**[2,4], **Carmella Evans-Molina**[3,6,7]

[1.] Department of Anatomy, Cell Biology, & Physiology (ACBP), Indiana University School of Medicine (IUSM), Indianapolis, IN 46202

[2.] Indiana Center for Musculoskeletal Health, IUSM

[3.] Department of Pediatrics, Indiana University School of Medicine (IUSM), Indianapolis, IN, 46202

[4.] Department of Biomedical Engineering, Indiana University-Purdue University at Indianapolis (IUPUI), IN, 46202

[5.] Department of Biochemistry & Molecular Biology, IUSM

[6.] Center for Diabetes and Metabolic Disease and the Wells Center for Pediatric Research, IUSM

[7.] Richard L. Roudebush VA Medical Center

Abstract

A bidirectional and complex relationship exists between bone and glycemia. Persons with type 2 diabetes (T2D) are at risk for bone loss and fracture, however, heightened osteoanabolism may ameliorate T2D-induced deficits in glycemia as bone-forming osteoblasts contribute to energy metabolism via increased glucose uptake and cellular glycolysis. Mice globally lacking Nuclear Matrix Protein 4 (Nmp4), a transcription factor expressed in all tissues and conserved between humans and rodents, are healthy and exhibit enhanced bone formation in response to anabolic osteoporosis therapies. To test whether loss of *Nmp4* similarly impacted bone deficits caused by diet induced obesity, male wild type (WT) and *Nmp4*$^{-/-}$ mice (8wks) were fed either low-fat diet (LFD) or high-fat diet (HFD) for 12wks. Endpoint parameters included bone architecture, structural and estimated tissue level mechanical properties, body weight/composition, glucose-stimulated insulin secretion, glucose tolerance, insulin tolerance and metabolic cage analysis. HFD diminished bone architecture and ultimate force and stiffness equally in both genotypes. Unexpectedly, the *Nmp4*$^{-/-}$ mice exhibited deficits in pancreatic β-cell function and were modestly glucose intolerant under normal diet conditions. Despite the β-cell deficits, the *Nmp4*$^{-/-}$ mice were less sensitive to HFD-induced weight gain, increases in % fat mass, and decreases

Corresponding authors: Joseph P Bidwell, jbidwell@iupui.edu, Depart. of ACBP, IUSM, Indianapolis, IN, 46202, Joseph M. Wallace, jmwalla@iupui.edu, Depart. of Biomedical Engineering, IUPUI, Indianapolis, IN, 46202, Carmella Evans-Molina, cevansmo@iu.edu, Center for Diabetes and Metabolic Disease, IUSM, Indianapolis, IN, 46202.

†currently at the Section of Endocrinology, Diabetes and Metabolism, Department of Medicine, The University of Chicago, Department of Medicine, Chicago IL, 60637

Disclosures: The authors have no conflicts of interest to declare that are relevant to the content of this article.

in glucose tolerance and insulin sensitivity. We conclude that *Nmp4* supports pancreatic β-cell function but suppresses peripheral glucose utilization, perhaps contributing to its suppression of induced skeletal anabolism. Selective disruption of *Nmp4* in peripheral tissues may provide a strategy for improving both induced osteoanabolism and energy metabolism in comorbid patients.

Keywords

bone mechanical properties; insulin secretion; Nmp4; pancreatic β cells; type 2 diabetes

INTRODUCTION:

Men and women with type 2 diabetes (T2D) have a significantly increased fracture risk[1–4]. T2D-associated insulin resistance impairs osteoblast differentiation and mineralized matrix formation[5–8]. Similarly, diet induced obesity has been associated with the degradation of bone matrix and diminished skeletal material properties[9–11]. Notably, derangements in the bone-pancreas feedback loop may contribute to this pathophysiology as there is a putative reciprocal relationship between bone and pancreatic β cells[12,13]. Briefly, during bone formation osteoblasts are metabolically reprogrammed toward aerobic glycolysis, which increases their glucose uptake from the blood contributing to the maintenance of normoglycemia[14–16]. Additionally, bone is the source of osteokines including undercarboxylated osteocalcin (unOCN) and lipocalin-2, which act as hormones and enhance pancreatic β cell function and insulin sensitivity in the peripheral tissues, although the role unOCN is controversial[12,17–23]. The release of insulin completes the bone-pancreas loop via its support of bone formation and matrix deposition[19,24].

Anabolic osteoblasts may resist the impact of T2D on bone phenotype because these cells improve global glucose metabolism via increased glucose uptake and cellular glycolysis[14–16]. We have engineered a mouse that exhibits a heightened capacity for induced skeletal anabolism[25–28]. Animals globally lacking *Nmp4* (Nuclear Matrix Protein 4, a.k.a. *ZNF384*, *Zfp384*, *Ciz)*, which is a Cys_2His_2 zinc finger transcription factor that is expressed in all tissues and is highly conserved between humans and rodents[29], are healthy and exhibit an unexceptional skeletal phenotype[30]. However, when challenged with the osteoanabolic parathyroid hormone (PTH), these mice exhibit enhanced bone formation with improved material properties compared to their wild type (WT) littermates[26–28,30,31].

Naïve *Nmp4*$^{-/-}$ mice harbor more bone marrow osteoprogenitors than WT mice and in culture these cells exhibit precocious and enhanced mineralization[27,28,31]. *Nmp4*$^{-/-}$ osteogenic cells have increased capacity for metabolic conversion to glycolysis[28] and express high levels of OCN[25–27], both proposed key traits necessary for regulating global energy utilization[16,32–34]. In addition, loss of *Nmp4* enhances bone cell ribosome biogenesis, expands the protein processing capacity of the endoplasmic reticulum, and upregulates glycolysis, which together converts osteoblasts into super-secretors of bone matrix proteins including osteocalcin[28,35]. To test whether *Nmp4*$^{-/-}$ bone is protected from metabolic stress we placed male *Nmp4*$^{-/-}$ and WT mice on high-fat or low-fat diet for 12wks and evaluated skeletal architecture, mechanical properties, and metabolic parameters.

Unexpectedly, we discovered that in addition to its role in regulating some aspects of bone physiology, *Nmp4* contributes to governing β cell insulin secretion and peripheral glucose utilization.

MATERIALS AND METHODS:

Mice:

Wild type (WT) and *Nmp4*$^{-/-}$ mice were maintained at Indiana University Bioresearch Facility School of Dentistry. The strategy for engineering the global *Nmp4*$^{-/-}$ animals has been described in detail previously[30]. Briefly, the approach comprised removal of coding exons 4 – 7 via homologous recombination. The appropriately modified embryonic stem (ES) cell lines from 129SvEv ES clones were microinjected into C57BL/6J blastocysts and the chimeric mice were crossbred with the C57BL/6J mice (The Jackson Laboratory, Bar Harbor, ME) to generate germline transmission. These mice were backcrossed for nine generations (N9) on the C57BL/6J background. The WT littermates were used as the control cohort. The mice were housed, 2–4 mice/cage, under a 12hr light/12hr dark regimen. Male WT and *Nmp4*$^{-/-}$ mice (8wks of age) were sorted into four treatment cohorts including (i) WT low fat diet (LFD); (ii) WT high fat diet (HFD); (iii) *Nmp4*$^{-/-}$ LFD; (iv) *Nmp4*$^{-/-}$ HFD. The mice were fed ad libitum either Teklad TD.88137 (adjusted calories diet 42% from fat) or the Teklad TD.05230 control diet. Treatment lasted 12wks (20wks of age). For baseline glycemia, insulinemia, and insulin sensitivity we also used N7 and N9 mice from ages 6–12wks of age. The Indiana University Institutional Animal Care and Use Committee approved all experimental procedures described in this study.

Micro-computed tomography (μCT):

Skeletal architecture was evaluated as previously described[28,36]. Briefly, femurs were dissected from the 20-week-old male mice, soaked in saline (0.9%), wrapped with gauze and stored at –20°C. The left femurs were brought to room temperature and scanned while hydrated with a 10 μm voxel size using a Skyscan 1172 μCT system (Bruker). Scans were performed using a 0.7-degree angle increment, two frames averaged, through a 0.5 mm Al filter (V = 60 kV, I = 167 μA). Images were reconstructed (nRecon) and calibrated to hydroxyapatite-mimicking phantoms (0.25 and 0.75 g/cm3 Ca-HA) for calculation of tissue mineral density (TMD). A 1mm trabecular region of interest (ROI) was selected in the distal metaphysis, starting at the most proximal location of the distal growth plate and extending proximally up the bone. Cancellous architecture was quantified using CT Analyzer (CTAn) and included bone volume fraction (BV/TV, %), trabecular number (Tb N, mm^{-1}), trabecular thickness (Tb Th, mm), trabecular spacing (Tb Sp, mm), and trabecular tissue mineral density, (Tb TMD mgHA/cm^3). A 1 mm cortical ROI was selected at approximately 50% length of the femur, then analyzed with a custom MATLAB (MathWorks, Inc. Natick, MA) program. Parameters obtained for femoral cortical bone included marrow area (mm^2), cortical area (mm^2), cortical thickness (mm), endocortical bone surface (BS) (mm), periosteal BS (mm), maximum moment of inertia (I_{max}, mm^4), minimum moment of inertia (I_{min}, mm^4).

Mechanical testing:

Left femurs from each mouse were thawed to room temperature and monotonically tested to failure in three-point bending at a displacement rate of 0.025 mm/sec using a support span of 8.3 mm[28,37]. Briefly, the femurs were oriented in the anterior-posterior direction with the anterior side in tension. The moment of inertia about the femoral medial-lateral axis and the extreme fiber in the anterior direction were obtained from the μCT images of the bone and were utilized to map load-displacement to stress-strain, using standard beam bending equations. Structural-level mechanical and tissue-level material properties were then derived from the stress-strain and load-displacement curves.

Metabolic Testing:

Body composition of WT and *Nmp4*$^{-/-}$ mice was evaluated by quantitative magnetic resonance imaging using EchoMRI Body Composition Analyzer (EchoMRI, LLC, Houston, Texas). Metabolic cage studies were performed using a TSE systems PhenoMaster Metabolism Research Platform (Chesterfield, MO) equipped with calorimetry, feeding/drinking, and activity monitoring[38]. Intraperitoneal glucose tolerance tests (IP-GTT) were performed subsequent to a 6hr fast and intraperitoneal injection of glucose at 1 g/kg; blood glucose levels were measured using an AlphaTRAK glucometer (Abbott Laboratories, Abbott Park, IL) at 0, 10, 20, 30, 60, 90, 120, and 180 min. To evaluate insulin sensitivity, insulin tolerance tests (ITT) were conducted by administering 0.75 U/kg insulin via IP injection after 2 hours fast and blood glucose levels were measured at times 0, 15, 30, 45, 60 minutes post insulin challenge. For β cell mass pancreata were processed, and insulin immunohistochemistry was performed as previously described[39]. Tissue sections, 3 per mouse (technical replicates for each biological replicate) and at least 50μm apart, were analyzed using Zen Blue software (Zeiss, Oberkochen, Germany). The insulin positive area in pixels were divided by the total pancreas area in pixels, and then multiplied by pancreas weight to generate β cell mass in mg.

Islet isolation and insulin secretion:

Pancreatic islets were isolated from WT and *Nmp4*$^{-/-}$ mice by collagenase digestion, hand-picked, and cultured in phenol-free low-glucose Dulbecco's modified Eagle's medium overnight prior to use[39,40]. Islets were preincubated at 37°C in Hank's balanced salt solution (HBSS) with 2.5 mM glucose for 2hrs. Cell medium was removed and replaced with fresh HBSS solution containing either 2.5 mM glucose and then incubated for an additional 1 hr. The cell medium was collected and HBSS supplemented with 15mM glucose was again added and incubated for 1 hr prior to medium collection Secreted insulin was measured by ELISA (Alpco, Salem, NH). Insulin secretion was normalized to the total insulin content of the cell extract[39]. To measure the acute in vivo β cell insulin secretory response to a glucose challenge, we performed separate experiments where mice were fasted overnight and then injected intraperitoneally with 2g/kg body weight of glucose. Serum was obtained at time 0, 2, and 10 min following glucose injection. Serum insulin levels were measured using an ultrasensitive mouse ELISA (Alpco). To generate transmission electron micrograph images, isolated islets were fixed in 2% glutaraldehyde and 4% paraformaldehyde in 0.1 mol/L sodium cacodylate buffer and transferred to the Advanced Electron Microscopy

Facility at the University of Chicago[41]. The relative percentages of mature, immature, and rod-like secretory granules were quantitated manually with ImageJ (NIH), Bethesda MD) as previously described[41].

Statistical analysis:

The JMP Version 15 (SAS Institute, Cary, NC), and Prism 9 (GraphPad Software, San Diego, CA) were used to process statistical analyses. A two-way ANOVA was employed to determine whether genotype or diet had an effect on bone architecture and mechanical parameters and to evaluate whether an interaction occurred between diet and genotype. When a significant main effect was found, all pairwise post hoc comparisons were conducted to identify significant intergroup differences. Those comparisons yielding p values ≤0.05, were reported. We used a repeated measures multivariate analysis of variance (MANOVA) to assess whether genotype or diet had a significant impact on body weight during the experimental period (8wks – 20wks of age), as well as well as to determine whether interaction occurred between the independent variables of genotype and diet. Briefly, a significant genotype x diet interaction indicated that the WT and *Nmp4*$^{-/-}$ mice responded differently to the same diet. A significant genotype x time interaction indicated that the WT and *Nmp4*$^{-/-}$ mice differed in the rate of body mass accrual over the entire experimental period. For some experiments, unpaired, two-tailed t-tests were employed as indicated. Additionally, a nested, mixed model ANOVA was used to compare WT and *Nmp4*$^{-/-}$ pancreatic β-cell mass. For non-parametric data the Wilcoxon test was used. Data are presented as means ± SD, and statistical significance was taken at p ≤0.05.

RESULTS:

HFD attenuates bone architecture and some mechanical properties in both WT and Nmp4$^{-/-}$ mice.

Male WT and *Nmp4*$^{-/-}$ mice (8wks of age) were maintained on LFD or HFD for 12wks (20wks of age) as described in the Material and Methods. There were four treatment groups: 1) WT LFD, 2) WT HFD, 3) *Nmp4*$^{-/-}$ LFD, and 4) *Nmp4*$^{-/-}$ HFD (n = 10/group). Femoral bone volume fraction (BV/TV, %) was significantly attenuated in mice of both genotypes in response to HFD. WT LFD cohorts exhibited a femoral BV/TV (%) of 26.5 ±4.10 vs. the WT HFD mice of 22.15±2.70, a decrease of 16%. The KO LFD cohorts exhibited a BV/TV (%) of 24.67 ±3.65 vs. the KO HFD mice of 19.51±1.18, a decrease of 19% (Figures 1A and 1B). Several other trabecular parameters were significantly attenuated in mice of both genotypes under the HFD regimen including Tb N, Tb Th, and Tb TMD (Table 1). Also, Tb Sp was increased in both HFD cohorts, i.e., the spaces between the trabeculae were enlarged (Table 1). The HFD treatment also attenuated femoral cortical thickness (mm) in both genotypes. The cortical thickness for WT LFD mice was 0.242 ±0.016 vs. 0.226 ±0.011 for the WT HFD group, a decrease of 7%. Similarly, the KO LFD cohorts exhibited a cortical thickness of 0.233±0.013 vs. 0.211±0.006 for the KO HFD mice, a decrease of 11% (Figure 1C). Similarly, several aspects of cortical geometry were decreased with HFD including cortical area, cortical thickness, periosteal BS, endocortical BS, I_{MAX}, and I_{MIN} (Table 1). A genotype effect was observed for all these parameters, showing a decrease in these values for the *Nmp4*$^{-/-}$ mice (Table 1). The two-way ANOVA showed main effects of

diet and genotype for several structural parameters but no diet x genotype interactions. To determine the intergroup differences giving rise to the significant main effects we conducted a Tukey's HSD for all pairwise comparisons for femoral BV/TV and femoral cortical thickness. This analysis showed no difference between the *Nmp4*$^{-/-}$ LFD and WT LFD and cohorts for femoral BV/TV (p=0.56) or cortical thickness (p=0.42), which is consistent with our previous published observations that *Nmp4*$^{-/-}$ mice have an unremarkable baseline skeletal phenotype[26–28,31]. This analysis also showed no difference between WT HFD and *Nmp4*$^{-/-}$ HFD cohorts for femoral BV/TV p=0.25. However, there was a small difference between WT HFD and *Nmp4*$^{-/-}$ HFD for cortical thickness that just reaches significance at p=0.04. We conclude that loss of *Nmp4* did not protect mice from HFD-induced bone loss.

The force-displacement (Figure 2A) and stress-strain (Figure 2B) curves qualitatively showed that both strength and stiffness were reduced with HFD (main effect of diet), reflective of a whole bone that is less resistant to fracture under an applied load and is consistent with a smaller bone overall. This size dependence is further supported since properties normalized for the difference in size (e.g. stress/strain), showed no differences at the tissue level. Post-yield behavior appeared unaffected by diet, suggesting both groups are able to tolerate damage similarly after yield is reached. Nevertheless, ultimate stress, which is the maximum strength of the bone at the material level, normalized for the bone geometry approached significance (p = 0.06, *Nmp4*$^{-/-}$ > WT, Table 2), consistent with our previous study evaluating female WT and *Nmp4*$^{-/-}$ mice under anabolic osteoporosis treatments[28]. Furthermore, Young's modulus a mechanical property that measures the stiffness of a solid material was significantly higher in the *Nmp4*$^{-/-}$ mice (p = 0.01, *Nmp4*$^{-/-}$ > WT, Table 2). This is consistent with an earlier study using female *Nmp4*$^{-/-}$ mice[28]. Consistent with the architectural results, the 3pt-bending derived data indicates that the *Nmp4*$^{-/-}$ mice were not impervious to any HFD-induced changes in estimated bone mechanical properties.

Nmp4$^{-/-}$ mice exhibit an intrinsic defect in β cell function and total body glucose homeostasis.

Nmp4 is expressed in all tissues and appears to regulate cell secretion[28,29,35]. For example, mice with whole body knockouts of *Nmp4* exhibit reduced cytokine/chemokine secretion by lung cells, macrophages, and joint cells during influenza infection and arthritis progression, reducing disease severity by minimizing inflammation[42,43]. Therefore, to evaluate pancreatic *β* cell function, we first evaluated baseline glycemia, insulinemia and insulin sensitivity of WT and *Nmp4*$^{-/-}$ mice and observed no differences between the genotypes (Figure 3A). We then performed IP-GTT on both genotypes (n=20/genotype) at 8wks of age as described in the Materials and Methods. When the area under the curve (AUC) was compared between the genotypes, the *Nmp4*$^{-/-}$ mice showed a ~17% increase in the AUC compared to the WT cohorts (p=0.0084 t-test, Figure 3B), with no significant difference in fasting blood glucose levels (data not shown).

EchoMRI was performed to determine baseline body composition of *Nmp4*$^{-/-}$ and WT mice at 8wks of age (n=15–17/genotype). The *Nmp4*$^{-/-}$ mice exhibited a modest reduction in body weight 22.59 ± 1.28g WT vs. 21.07 ± 1.98g *Nmp4*$^{-/-}$ (p=0.02, t-test, Figure 3C, first panel). However, they also showed a small increase in % body fat 5.34 ± 0.99% WT vs. 7.47

± 1.97% *Nmp4*$^{-/-}$ (p=0.0009, t-test, Figure 3C, second panel) and lower lean mass 20.42 ± 1.45g WT vs. 18.37 ± 1.60g *Nmp4*$^{-/-}$ (p= 0.001, t-test, Figure 3C, third panel).

Nmp4 is expressed in all tissues[29]. Since *Nmp4*$^{-/-}$ mice exhibited mild glucose intolerance without differences in insulin sensitivity, we interrogated pancreatic β cell mass and function in our global knockout mice. Immunohistochemical analysis of WT and *Nmp4*$^{-/-}$ pancreatic sections from 8wk-old male mice revealed a trend towards reduced β cell mass (p=0.06, Figure 3D, first and second panels). To ascertain whether *Nmp4* influences β cell insulin secretion we isolated islets from our WT and *Nmp4*$^{-/-}$ mice and performed static glucose-stimulated insulin secretion (GSIS) assays as described in Materials and Methods. Insulin release in response to glucose stimulation was significantly attenuated in islets from *Nmp4*$^{-/-}$ mice compared to those islets obtained from WT littermates (Figure 3D, fourth panel).

Transmission EM images of islet β-cells isolated from WT and *Nmp4*$^{-/-}$ mice revealed no observable change in insulin granule morphology (Figure 4). WT and *Nmp4*$^{-/-}$ mice exhibited no differences in the percent of mature secretory granules characterized by an electron-dense core and a translucent halo appearance. Similarly, there was no difference in the percent immature granules distinguished by their gray low-dense appearance (Figure 4). Interestingly, the *Nmp4*$^{-/-}$ islets showed a significant increase in atypical granules with a rod-shaped core (Figure 4). Taken together, these data suggest lower lean mass as well as reductions in β-cells function may contribute to reduced glucose tolerance in *Nmp4*$^{-/-}$ mice.

Nmp4$^{-/-}$ mice are less sensitive to HFD-induced weight gain and attendant changes in global glucose homeostasis

Despite the deficits in baseline glucose metabolism, and a slight increase in fat mass, the *Nmp4*$^{-/-}$ were not as susceptible to HFD-induced weight gain as their WT littermates (n= 10/cohort, Figure 5). Analysis of the longitudinal data indicated a strong genotype effect (p=0.0021, Figure 5), showing that the WT mice weighed more than the *Nmp4*$^{-/-}$ mice throughout the feeding period. There was a significant treatment effect (p=0.0210, Figure 5) confirming that mice on the HFD gained more weight than the cohorts on the LFD. Although there was no significant genotype x treatment interaction (p=0.7225, Figure 5), i.e., the WT and *Nmp4*$^{-/-}$ mice both gained weight on the HFD, there was a significant genotype x time interaction (p=0.0079, Figure 5) meaning the *Nmp4*$^{-/-}$ mice exhibited a significantly slower rate of weight gain than the WT mice.

WT mice exhibited the expected decrease in glucose tolerance on the HFD vs. LFD whereas the *Nmp4*$^{-/-}$ mice showed no change (Figure 6A). Specifically, IP-GTT were performed after 12wks of HFD/LFD treatment (20wks of age) on all four cohorts (n=10/cohort). When the AUC was compared between groups, the WT HFD mice showed a 28% increase in the AUC compared to their WT LFD cohorts consistent with a significant decrease in glucose tolerance (p= 0.0018, 1W ANOVA, Tukey's HSD, Figure 6A). Consistent with their reduced weight gain, the *Nmp4*$^{-/-}$ HFD mice exhibited only a 10% increase in AUC compared to the *Nmp4*$^{-/-}$ LFD cohorts, which did not reach statistical significance (p = 0.3429 Figure 6A). Interestingly comparison between WT LFD and *Nmp4*$^{-/-}$ LFD at 20wks of age showed that the AUC for the *Nmp4*$^{-/-}$ mice was about 21% larger (p= 0.0239, Figure 6A). This is nearly

identical to the 17% increase in the IP-GTT AUC values comparing WT and *Nmp4*$^{-/-}$ baseline at 8wks of age (Figure 3B).

Both WT and *Nmp4*$^{-/-}$ mice showed a decrease in insulin sensitivity on the HFD vs. LFD but the *Nmp4*$^{-/-}$ mice were significantly less affected by the HFD challenge (Figure 6B). Specifically, ITT were performed after 12wks of HFD/LFD treatment (20wks of age) on all four cohorts. When the AUC was compared between groups, the WT HFD mice showed a 62% increase in the AUC compared to their WT LFD cohorts consistent with a significant decrease in insulin sensitivity ($p<0.0001$ Figure 6B). The *Nmp4*$^{-/-}$ HFD mice exhibited 40% increase in AUC compared to their LFD cohorts, which was significant ($p = 0.0077$ Figure 6B). However, the AUC of *Nmp4*$^{-/-}$ HFD was significantly smaller than that of the WT HFD cohorts ($p=0.0245$, Figure 6B) indicating that the *Nmp4*$^{-/-}$ mice on HFD were more insulin sensitive than the WT mice. Interestingly, comparison between WT LFD and *Nmp4*$^{-/-}$ LFD at 20wks of age showed no significant difference ($p= 0.8989$, Figure 6B). This is consistent with their baseline insulin sensitivity status at 8wks of age.

Finally, Echo MRI showed that *Nmp4*$^{-/-}$ mice were less sensitive to gains in body mass and %fat mass on the HFD compared to the WT mice. Consistent with our longitudinal study, Echo MRI showed about a 21% increase in body mass between the WT LFD and WT HFD mice at the end of the study ($p=0.0001$, Figure 6C). The *Nmp4*$^{-/-}$ mice exhibited a 12% increase between the LFD and HFD cohorts that was not significant ($p=0.0747$, Figure 6C, first panel). There was no significance difference in body mass between the WT and *Nmp4*$^{-/-}$ LFD cohorts at the end of the study ($p=0.0824$, Figure 6C).

Both genotypes showed an increase in %fat mass on the HFD. The WT on LFD exhibited a 14.77 ± 5.07% fat mass at the end of the study compared to their WT cohorts on HFD of 32.10 ± 4.87% fat mass ($p<0.0001$, Figure 6C, second panel). The *Nmp4*$^{-/-}$ mice on LFD had a 13.02 ± 3.79% fat mass at the end of the study vs. the HFD *Nmp4*$^{-/-}$ cohorts of 24.84± 6.51% ($p<0.0001$, Figure 6C, second panel). This HFD-associated %fat mass in the *Nmp4*$^{-/-}$ mice was significantly lower than that of the WT HFD cohorts ($p=0.0165$, Figure 6C, second panel). Diet had no effect on lean mass of either genotype, which was modestly lower in the *Nmp4*$^{-/-}$ mice than the WT animals on both regimens.

We next explored the effect of *Nmp4* on insulin secretion under 12wks of LFD and HFD using an in vivo GSIS assay. Consistent with our ex vivo experiments, *Nmp4*$^{-/-}$ mice on LFD displayed decreased circulating insulin compared to their WT LFD cohorts (Figures 7A & 7B). Interestingly, HFD did not further exacerbate the attenuated glucose-induced insulin secretion in the *Nmp4*$^{-/-}$ mice but significantly lowered this response in the WT HFD group (Figures 7A and 7B). Taken together, we conclude that under metabolic challenge the significantly diminished insulin secretion in global *Nmp4*$^{-/-}$ mice is compensated by the response of the peripheral tissues.

Nmp4$^{-/-}$ mice are more sensitive to HFD-induced changes in activity

To examine the influence of *Nmp4* on metabolic, behavioral, and physiological parameters, we next pursued metabolic cage studies. WT and global *Nmp4*$^{-/-}$ mice were maintained on LFD or HFD as described in Materials and Methods. Loss of *Nmp4* did not alter the

respiratory exchange ratio (RER, ratio of CO_2 produced to O_2 consumed) compared to WT mice (Figure 8A). Mice on the LFD exhibited an RER of ~0.85 (day) – 0.95 (night) whereas mice on the HFD showed an RER of 0.75 (day) – 0.90 (night). These results are consistent with the idea that the predominant fuel source of mice on the control diet was carbohydrates, while the fuel source was a mixture of both fat and carbohydrate for mice on the HFD. There was no difference in mouse activity between the genotypes on the LFD but the *Nmp4*$^{-/-}$ HFD mice were less active than their WT littermates on HFD (Figure 8B). Additionally, the HFD *Nmp4*$^{-/-}$ mice consumed less food at night than their WT HFD cohorts (Figure 8C). This prompted the question as to whether the Nmp4$^{-/-}$ phenotype is in general associated with a difference in food consumption. Total food consumption on the LFD diet showed a near significant greater consumption in the *Nmp4*$^{-/-}$ mice. WT LFD cohorts (day+night) consumed a total (grams) of 4.75 ±0.50 vs. 5.68±0.65 for *Nmp4*$^{-/-}$ LFD (day+night), p=0.06, two-tailed t-test. Total food consumption on the HFD diet showed no difference between the genotypes. WT HFD cohorts (day+night) consumed a total (grams) of 4.88 ±0.53 vs. 4.07±0.56 for *Nmp4*$^{-/-}$ HFD (day+night), p=0.08, two-tailed t-test. Similarly, total food consumption i.e., LFD+HFD showed no difference between the genotypes. WT LFD+HFD cohorts (day+night) consumed a total (grams) of 9.62 ±0.17 vs. 9.75±1.16 for *Nmp4*$^{-/-}$ LFD+HFD (day+night), p=0.83, two-tailed t-test. We conclude that *Nmp4* has an impact on activity and some aspects of feeding behavior during metabolic challenge.

DISCUSSION:

In the present study we inquired whether mice globally lacking *Nmp4* are protected from HFD-induced bone loss and mechanical deficits. Bone remodeling is a significant glucose-consuming process[44–47]. Glucose uptake and utilization by bone cells contributes to the regulation of global energy metabolism, is governed by insulin, and is influenced by perturbations in whole-body metabolism[14–16,44,45]. Additionally, bone may release factors during remodeling that support pancreatic β-cell function and improve peripheral tissue insulin sensitivity. In turn insulin feeds back and supports bone formation[12,17–23]. One of these purported osteokines is undercarboxylated osteocalcin, although this is controversial[12,17–23]. PTH-induced anabolic bone remodeling is fueled by glucose and osteoblasts activated by PTH suppress glucose entry into the TCA cycle and divert it towards glycolysis[48]. Indeed, pharmacological inhibition of glycolysis suppresses PTH anabolic action[48]. *Nmp4*$^{-/-}$ mice exhibit PTH-induced enhanced bone formation compared to their WT littermates[25–28,30,31]. Our recent studies indicate that the exaggerated PTH-mediated increase in *Nmp4*$^{-/-}$ bone is driven by a boost in bone formation, not a decrease in bone resorption[26,27]. This phenomenon appears to be mediated by an increase in the number of hyper-anabolic osteoprogenitors that exhibit an enhanced capacity for glucose uptake and glycolysis[26–28,31]. Indeed, preliminary data show that conditional loss of *Nmp4* from MSPCs recapitulates the PTH-induced skeletal phenotype observed in the global knockout mice[49]. *Nmp4*$^{-/-}$ osteoblasts express strikingly high levels of osteocalcin[25,26,28] and *Nmp4*$^{-/-}$ mice exhibit an enhanced PTH-induced elevation of serum osteocalcin compared to their WT littermates[25,27], perhaps serving as a tonic to the pancreatic β-cells[20]. The rationale underlying this investigation is that the unique *Nmp4*$^{-/-}$ skeletal phenotype might act to shield from the HFD-induced bone deficits.

However, our results showed that the *Nmp4*$^{-/-}$ mice were not resistant to HFD-induced changes in bone architecture, perhaps due, in part, to the absence of the PTH cue to activate the amplified osteoanabolic phenotype. Both WT and *Nmp4*$^{-/-}$ mice showed significant HFD-associated decreases in several architectural bone parameters including trabecular BV/TV, TbN, TbTh, TbSp, and cortical area, thickness, periosteal BS, endocortical BS, I_{max} and I_{min}. HFD altered some femoral bone mechanical properties in both WT and *Nmp4*$^{-/-}$ mice. Although we did not perform bone histomorphometry our treatment regimen was nearly identical to that of a recent study by Tencerova et al., 2018, using WT male C57BL6J mice showing that diet-induced obesity decreased bone formation and matrix apposition rates with no impact on bone resorption[50]. Similarly, Ross et al., 2021, showed an HFD-associated decrease in bone formation in C57BL6J mice (8 weeks −18 weeks of age)[51]. Therefore, treating *Nmp4*$^{-/-}$ mice with PTH or another anabolic trigger might be necessary to abrogate bone loss during the metabolic challenge. Indeed, PTH and PTHrp are efficacious in reducing fractures and improving BMD in osteoporotic patients with T2D[52,53].

A novel discovery of the present study is that *Nmp4* regulates pancreatic β cell function and potentially development, and to our knowledge this is the first evidence that these cells require this novel transcription factor for optimum activity. The *Nmp4*$^{-/-}$ mice were modestly glucose intolerant in the absence of metabolic challenge at both 8wks and at 20wks of age. Pancreatic β cell mass and response to *in vitro* glucose challenge (GSIS) were decreased in the *Nmp4*$^{-/-}$ tissue. The increased number of atypical granules with rod-like dense cores like those observed in the *Nmp4*$^{-/-}$ pancreatic sections, are thought to be indicative of defects in insulin crystallization, packaging, and secretion contributing to glucose intolerance[54–56], which is consistent the attenuated insulin secretion of the *Nmp4*$^{-/-}$ mice. Like the observed reduction in insulin secretion, loss of *Nmp4* attenuates chemokine expression and release in mouse lung epithelial cells and bone-marrow-derived macrophages, contributing to decreased H1N1 morbidity[42]. Conversely, loss of *Nmp4* increases collagen secretion in osteoprogenitors[28,35]. RNA-seq and biochemical analyses of osteoprogenitors show that Nmp4 regulates over 5000 genes in these cells and includes pathways controlling ribosome biogenesis and tRNA charging (protein production) and the unfolded protein response (protein delivery) consistent with Nmp4 control of secretory cell activity[28,35]. Some of the many target genes along these pathways that are transcriptionally regulated by Nmp4 include and *c-Myc*, *Ak6*, *Tcof1* (ribosome biogenesis), *Nars, Yars, Eprs* (tRNA charging), and *Gadd34*, *Ddit3/Chop*, *Atf6* (unfolded protein response)[26,28]. Thus, we conclude *Nmp4* regulates the machinery of professional secretory cells in a tissue-specific manner. Further studies will be required to pinpoint the precise molecular pathways through which *Nmp4* regulates β cell health.

Remarkably, the β cell deficits notwithstanding, the *Nmp4*$^{-/-}$ mice exhibited a significantly slower rate of HFD-associated weight gain and decline in glucose metabolism as compared to the WT mice. Although, HFD increased fat mass in both WT and *Nmp4*$^{-/-}$ mice, the *Nmp4*$^{-/-}$ mice had significantly less fat gain. All of this may have contributed to the fact that the WT mice exhibited a decrease in glucose tolerance on the HFD vs. LFD whereas the *Nmp4*$^{-/-}$ mice showed no such change. Absence of *Nmp4* intrinsically affects pancreatic β-cells and insulin secretion and induces glucose intolerance. This may explain

why *Nmp4*$^{-/-}$ mice are not more glucose intolerant when fed with HFD. However, although both WT and *Nmp4*$^{-/-}$ mice showed a decrease in insulin sensitivity on the HFD vs. LFD the *Nmp4*$^{-/-}$ mice were significantly less affected by this metabolic challenge. A reasonable inference is that *Nmp4*$^{-/-}$ peripheral tissues (liver, muscle, bone) take up more glucose when presented with a metabolic challenge. *Nmp4*$^{-/-}$ mesenchymal stem progenitors/osteoprogenitors exhibit an enhanced capacity for glucose uptake and glycolysis, which fuels bone formation[28]. Nmp4 transcriptionally regulates several genes in the glycolytic pathway including *Eno3*, *Pdk1*, and *Pkm*[28]. This may explain the enhanced insulin sensitivity in the *Nmp4*$^{-/-}$ mice post HFD diet. However, the *Nmp4*$^{-/-}$ osteoprogenitors may require the PTH anabolic cue to further enhance insulin sensitivity and resist bone deficits under the HFD regimen. Finally, adipocytes are derived from mesenchymal stem/progenitor cells[57] thus *Nmp4*$^{-/-}$ fat tissue may exhibit a similar enhanced glycolytic phenotype. We conclude that *Nmp4* supports pancreatic β-cell function but suppresses peripheral glucose utilization, perhaps contributing to its anti-osteoanabolic activity.

The relationships among bone physiology, obesity, and energy/glucose metabolism are areas of intense investigation and include the search for genes that may link bone anabolism and global energy metabolism. The present data shows that a single gene governing the capacity of induced bone anabolism, is a regulatory factor in pancreatic beta cell insulin secretion and influences peripheral glucose utilization. We have recently engineered an *Nmp4*-floxed mouse, which will allow us to further examine these potential novel connections and may be a useful preclinical model for exploring therapeutic strategies targeting osteoporosis and T2D comorbidities.

Acknowledgements:

This work was supported by National Institutes of Health Grants 1R01 AR073739 to J.P.B. and R01 DK093954 and VA Merit Award I01BX001733 (to C.E-M.). The authors would also like to thank The Center for Diabetes & Metabolic Diseases Islet & Physiology Core (P30DK097512) and for performing metabolic assays, islet isolations, and body composition analysis.

REFERENCES:

1. Melton LJ 3rd, Leibson CL, Achenbach SJ, Therneau TM, Khosla S Fracture risk in type 2 diabetes: update of a population-based study. Journal of bone and mineral research : the official journal of the American Society for Bone and Mineral Research 2008;23:1334–42.
2. Bonds DE, Larson JC, Schwartz AV, et al. Risk of fracture in women with type 2 diabetes: the Women's Health Initiative Observational Study. The Journal of clinical endocrinology and metabolism 2006;91:3404–10. [PubMed: 16804043]
3. Tebe C, Martinez-Laguna D, Carbonell-Abella C, et al. The association between type 2 diabetes mellitus, hip fracture, and post-hip fracture mortality: a multi-state cohort analysis. Osteoporosis international : a journal established as result of cooperation between the European Foundation for Osteoporosis and the National Osteoporosis Foundation of the USA 2019;30:2407–15.
4. Yilmaz V, Umay E, Gundogdu I, Tezel N. Effect of type 2 diabetes mellitus on treatment outcomes of patients with postmenopausal osteoporosis: a retrospective study. J Diabetes Metab Disord 2018;17:181–7. [PubMed: 30918853]
5. Hamann C, Goettsch C, Mettelsiefen J, et al. Delayed bone regeneration and low bone mass in a rat model of insulin-resistant type 2 diabetes mellitus is due to impaired osteoblast function. American journal of physiology Endocrinology and metabolism 2011;301:E1220–8. [PubMed: 21900121]

6. Kawashima Y, Fritton JC, Yakar S, et al. Type 2 diabetic mice demonstrate slender long bones with increased fragility secondary to increased osteoclastogenesis. Bone 2009;44:648–55. [PubMed: 19150422]
7. Weinberg E, Maymon T, Weinreb M. AGEs induce caspase-mediated apoptosis of rat BMSCs via TNFalpha production and oxidative stress. Journal of molecular endocrinology 2014;52:67–76. [PubMed: 24198288]
8. Villarino ME, Sanchez LM, Bozal CB, Ubios AM. Influence of short-term diabetes on osteocytic lacunae of alveolar bone. A histomorphometric study. Acta odontologica latinoamericana : AOL 2006;19:23–8. [PubMed: 17121195]
9. Ionova-Martin SS, Do SH, Barth HD, et al. Reduced size-independent mechanical properties of cortical bone in high-fat diet-induced obesity. Bone 2010;46:217–25. [PubMed: 19853069]
10. Ionova-Martin SS, Wade JM, Tang S, et al. Changes in cortical bone response to high-fat diet from adolescence to adulthood in mice. Osteoporosis international : a journal established as result of cooperation between the European Foundation for Osteoporosis and the National Osteoporosis Foundation of the USA 2011;22:2283–93.
11. Karim L, Bouxsein ML. Effect of type 2 diabetes-related non-enzymatic glycation on bone biomechanical properties. Bone 2016;82:21–7. [PubMed: 26211993]
12. Shi J, Fan J, Su Q, Yang Z. Cytokines and Abnormal Glucose and Lipid Metabolism. Frontiers in endocrinology 2019;10:703. [PubMed: 31736870]
13. Faienza MF, Luce V, Ventura A, et al. Skeleton and glucose metabolism: a bone-pancreas loop. International journal of endocrinology 2015;2015:758148. [PubMed: 25873957]
14. Dirckx N, Tower RJ, Mercken EM, et al. Vhl deletion in osteoblasts boosts cellular glycolysis and improves global glucose metabolism. The Journal of clinical investigation 2018;128:1087–105. [PubMed: 29431735]
15. Guntur AR, Gerencser AA, Le PT, et al. Osteoblast-like MC3T3-E1 Cells Prefer Glycolysis for ATP Production but Adipocyte-like 3T3-L1 Cells Prefer Oxidative Phosphorylation. Journal of bone and mineral research : the official journal of the American Society for Bone and Mineral Research 2018.
16. Karner CM, Long F. Glucose metabolism in bone. Bone 2017.
17. Clemens TL, Karsenty G. The osteoblast: an insulin target cell controlling glucose homeostasis. Journal of bone and mineral research : the official journal of the American Society for Bone and Mineral Research 2011;26:677–80.
18. Ferron M, Wei J, Yoshizawa T, et al. Insulin signaling in osteoblasts integrates bone remodeling and energy metabolism. Cell 2010;142:296–308. [PubMed: 20655470]
19. Fulzele K, Riddle RC, DiGirolamo DJ, et al. Insulin receptor signaling in osteoblasts regulates postnatal bone acquisition and body composition. Cell 2010;142:309–19. [PubMed: 20655471]
20. Tangseefa P, Martin SK, Fitter S, Baldock PA, Proud CG, Zannettino ACW. Osteocalcin-dependent regulation of glucose metabolism and fertility: Skeletal implications for the development of insulin resistance. Journal of cellular physiology 2018;233:3769–83. [PubMed: 28834550]
21. Lee NK, Sowa H, Hinoi E, et al. Endocrine regulation of energy metabolism by the skeleton. Cell 2007;130:456–69. [PubMed: 17693256]
22. Diegel CR, Hann S, Ayturk UM, et al. An osteocalcin-deficient mouse strain without endocrine abnormalities. PLoS genetics 2020;16:e1008361. [PubMed: 32463812]
23. Karsenty G The facts of the matter: What is a hormone? PLoS genetics 2020;16:e1008938. [PubMed: 32589668]
24. Wang X, Zhang G, Qi F, et al. Enhanced bone regeneration using an insulin-loaded nano-hydroxyapatite/collagen/PLGA composite scaffold. Int J Nanomedicine 2018;13:117–27.
25. Childress P, Philip BK, Robling AG, et al. Nmp4/CIZ suppresses the response of bone to anabolic parathyroid hormone by regulating both osteoblasts and osteoclasts. Calcified tissue international 2011;89:74–89. [PubMed: 21607813]
26. Childress P, Stayrook KR, Alvarez MB, et al. Genome-Wide Mapping and Interrogation of the Nmp4 Antianabolic Bone Axis. Molecular endocrinology 2015;29:1269–85. [PubMed: 26244796]

27. Shao Y, Hernandez-Buquer S, Childress P, et al. Improving Combination Osteoporosis Therapy In a Preclinical Model of Heightened Osteoanabolism. Endocrinology 2017;158:2722–40. [PubMed: 28637206]
28. Shao Y, Wichern E, Childress PJ, et al. Loss of Nmp4 optimizes osteogenic metabolism and secretion to enhance bone quality. American journal of physiology Endocrinology and metabolism 2019;316:E749–e72. [PubMed: 30645175]
29. Thunyakitpisal P, Alvarez M, Tokunaga K, et al. Cloning and functional analysis of a family of nuclear matrix transcription factors (NP/NMP4) that regulate type I collagen expression in osteoblasts. Journal of bone and mineral research : the official journal of the American Society for Bone and Mineral Research 2001;16:10–23.
30. Robling AG, Childress P, Yu J, et al. Nmp4/CIZ suppresses parathyroid hormone-induced increases in trabecular bone. Journal of cellular physiology 2009;219:734–43. [PubMed: 19189321]
31. He Y, Childress P, Hood M Jr., et al. Nmp4/CIZ suppresses the parathyroid hormone anabolic window by restricting mesenchymal stem cell and osteoprogenitor frequency. Stem cells and development 2013;22:492–500. [PubMed: 22873745]
32. Lee SY, Long F. Notch signaling suppresses glucose metabolism in mesenchymal progenitors to restrict osteoblast differentiation. The Journal of clinical investigation 2018;128:5573–86. [PubMed: 30284985]
33. Lacombe J, Al Rifai O, Loter L, et al. Measurement of bioactive osteocalcin in humans using a novel immunoassay reveals association with glucose metabolism and beta-cell function. American journal of physiology Endocrinology and metabolism 2020;318:E381–e91. [PubMed: 31935114]
34. Le Doan V, Marcil V. [Osteocalcin and glucose metabolism: assessment of human studies]. Med Sci (Paris) 2017;33:417–22. [PubMed: 28497738]
35. Young SK, Shao Y, Bidwell JP, Wek RC. Nuclear Matrix Protein 4 is a Novel Regulator of Ribosome Biogenesis and Controls the Unfolded Protein Response Via Repression of Gadd34 Expression. The Journal of biological chemistry 2016.
36. Powell KM, Brown AP, Skaggs CG, et al. 6'-Methoxy Raloxifene-analog enhances mouse bone properties with reduced estrogen receptor binding. Bone reports 2020;12:100246. [PubMed: 32016137]
37. Bart ZR, Hammond MA, Wallace JM. Multi-scale analysis of bone chemistry, morphology and mechanics in the oim model of osteogenesis imperfecta. Connective tissue research 2014;55 Suppl 1:4–8. [PubMed: 25158170]
38. Sims EK, Hatanaka M, Morris DL, et al. Divergent compensatory responses to high-fat diet between C57BL6/J and C57BLKS/J inbred mouse strains. American journal of physiology Endocrinology and metabolism 2013;305:E1495–511. [PubMed: 24169046]
39. Evans-Molina C, Robbins RD, Kono T, et al. Peroxisome proliferator-activated receptor gamma activation restores islet function in diabetic mice through reduction of endoplasmic reticulum stress and maintenance of euchromatin structure. Mol Cell Biol 2009;29:2053–67. [PubMed: 19237535]
40. Stull ND, Breite A, McCarthy R, Tersey SA, Mirmira RG. Mouse islet of Langerhans isolation using a combination of purified collagenase and neutral protease. Journal of visualized experiments : JoVE 2012.
41. Tong X, Kono T, Anderson-Baucum EK, et al. SERCA2 Deficiency Impairs Pancreatic beta-Cell Function in Response to Diet-Induced Obesity. Diabetes 2016;65:3039–52. [PubMed: 27489309]
42. Yang S, Adaway M, Du J, et al. NMP4 regulates the innate immune response to influenza A virus infection. Mucosal Immunol 2020.
43. Nakamoto T, Izu Y, Kawasaki M, et al. Mice Deficient in CIZ/NMP4 Develop an Attenuated Form of K/BxN-Serum Induced Arthritis. Journal of cellular biochemistry 2016;117:970–7. [PubMed: 26378628]
44. Zoch ML, Abou DS, Clemens TL, Thorek DL, Riddle RC. In vivo radiometric analysis of glucose uptake and distribution in mouse bone. Bone research 2016;4:16004. [PubMed: 27088042]
45. Wei J, Shimazu J, Makinistoglu MP, et al. Glucose Uptake and Runx2 Synergize to Orchestrate Osteoblast Differentiation and Bone Formation. Cell 2015;161:1576–91. [PubMed: 26091038]

46. Yang YY, Zhou YM, Xu JZ, et al. Lgr4 promotes aerobic glycolysis and differentiation in osteoblasts via the canonical Wnt/β-catenin pathway. Journal of bone and mineral research : the official journal of the American Society for Bone and Mineral Research 2021.
47. Regan JN, Lim J, Shi Y, et al. Up-regulation of glycolytic metabolism is required for HIF1alpha-driven bone formation. Proceedings of the National Academy of Sciences of the United States of America 2014;111:8673–8. [PubMed: 24912186]
48. Esen E, Lee SY, Wice BM, Long F. PTH Promotes Bone Anabolism by Stimulating Aerobic Glycolysis via IGF Signaling. Journal of bone and mineral research : the official journal of the American Society for Bone and Mineral Research 2015;30:1959–68.
49. Atkinson E, Adaway M, Korff C, et al. Conditional Loss of Nmp4 In Mesenchymal Stem Progenitor Cells Enhances PTH-Induced Bone Formation. JOURNAL OF BONE AND MINERAL RESEARCH; 2020: WILEY 111 RIVER ST, HOBOKEN 07030–5774, NJ USA. p. 136-.
50. Tencerova M, Figeac F, Ditzel N, Taipaleenmäki H, Nielsen TK, Kassem M. High-Fat Diet-Induced Obesity Promotes Expansion of Bone Marrow Adipose Tissue and Impairs Skeletal Stem Cell Functions in Mice. Journal of bone and mineral research : the official journal of the American Society for Bone and Mineral Research 2018;33:1154–65.
51. Ross DS, Yeh TH, King S, et al. Distinct Effects of a High Fat Diet on Bone in Skeletally Mature and Developing Male C57BL/6J Mice. Nutrients 2021;13. [PubMed: 35010888]
52. Schwartz AV, Pavo I, Alam J, et al. Teriparatide in patients with osteoporosis and type 2 diabetes. Bone 2016;91:152–8. [PubMed: 27374026]
53. Dhaliwal R, Hans D, Hattersley G, et al. Abaloparatide in Postmenopausal Women With Osteoporosis and Type 2 Diabetes: A Post Hoc Analysis of the ACTIVE Study. JBMR Plus 2020;4:e10346. [PubMed: 32258965]
54. Carrat GR, Haythorne E, Tomas A, et al. The type 2 diabetes gene product STARD10 is a phosphoinositide-binding protein that controls insulin secretory granule biogenesis. Molecular metabolism 2020;40:101015. [PubMed: 32416313]
55. Wijesekara N, Dai FF, Hardy AB, et al. Beta cell-specific Znt8 deletion in mice causes marked defects in insulin processing, crystallisation and secretion. Diabetologia 2010;53:1656–68. [PubMed: 20424817]
56. Nicolson TJ, Bellomo EA, Wijesekara N, et al. Insulin storage and glucose homeostasis in mice null for the granule zinc transporter ZnT8 and studies of the type 2 diabetes-associated variants. Diabetes 2009;58:2070–83. [PubMed: 19542200]
57. Pittenger MF, Mackay AM, Beck SC, et al. Multilineage potential of adult human mesenchymal stem cells. Science 1999;284:143–7. [PubMed: 10102814]

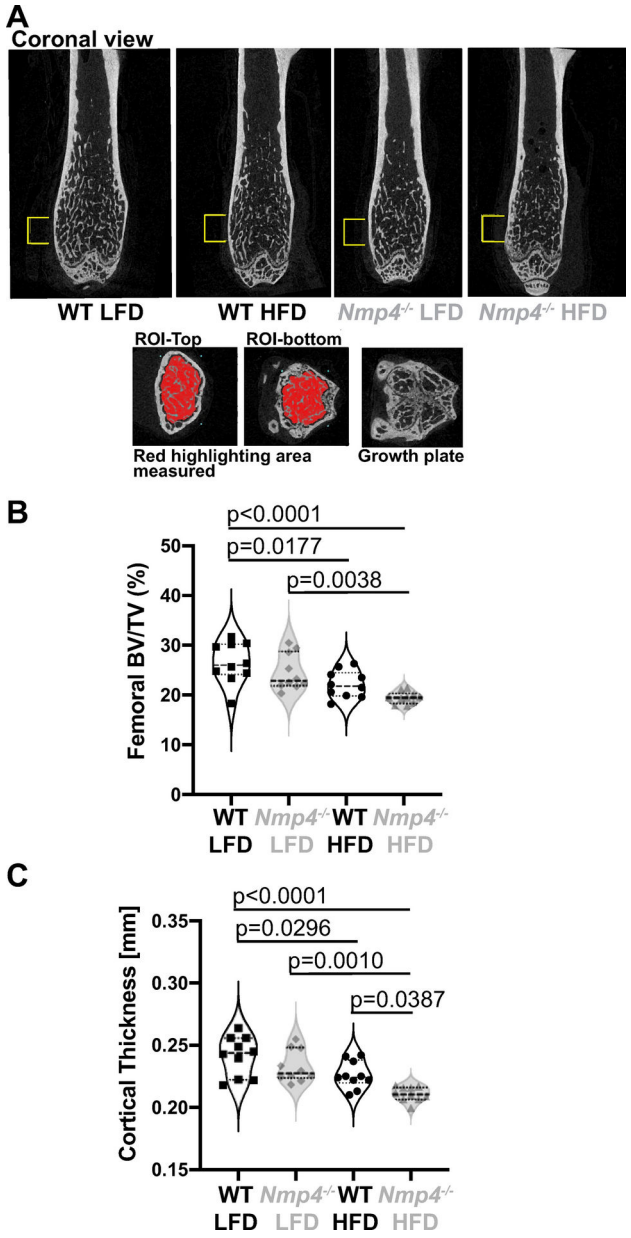

Figure 1: µCT analysis shows that HFD induces bone loss in both WT and *Nmp4*$^{-/-}$ mice.

[A] µCT images (coronal and cross-section) showing the femoral region of interest (ROI) starting above the growth plate and continuing for 1 mm so the growth plate would not be included within the analysis. The coronal images are from mice representing the femoral median BV/TV values from each of the four treatment cohorts. Cross-section image of the growth plate is also shown. **[B]** Distal femur trabecular BV/TV [%] of WT and *Nmp4*$^{-/-}$ mice on LFD or HFD for 12 wks from 8 wks – 20 wks of age. **[C]** Femoral cortical thickness from the same experimental mice. Statistical analyses: Two-way ANOVAs were performed using diet and genotype as main effects. The results of this analysis follow: femoral BV/TV [%]: Genotype p=0.03, Treatment p<0.0001, GxT p=0.68; femoral cortical thickness [mm] Genotype p=0.004, Treatment p<0.0001, GxT p=0.38. When a significant

main effect was indicated, all pairwise post hoc comparisons were conducted to identify intergroup differences. Those comparisons yielding p values ≤ 0.05, are indicated in the panel. Data represent average ± SD; n = 10 mice/group.

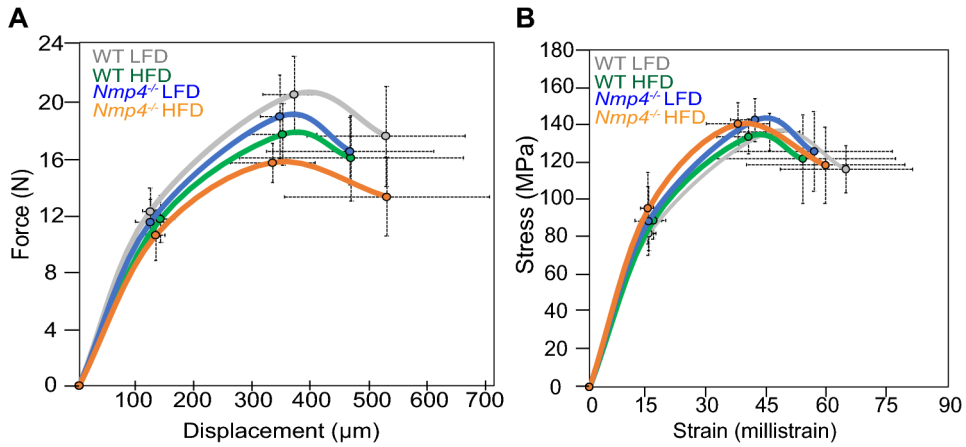

Figure 2: High fat diet induces changes in estimated bone mechanical properties in both WT and *Nmp4*$^{-/-}$ mice.

[A & B] Schematic representation of the mechanical responses of femurs obtained from the four cohorts at 20wks of age after 8wks of diet treatment including WT low fat diet (LFD); WT high fat diet (HFD); *Nmp4*$^{-/-}$ LFD; *Nmp4*$^{-/-}$ HFD. Each point represents the mean for each group (e.g., mean yield force and displacement to yield). The error bars are the standard error of the mean (SEM), n = 10 mice/group. **[A]** Relationship between force (N) and displacement (mm). **[B]** Relationship between stress (Mpa) and strain (mstrain). Also see data in Table 2

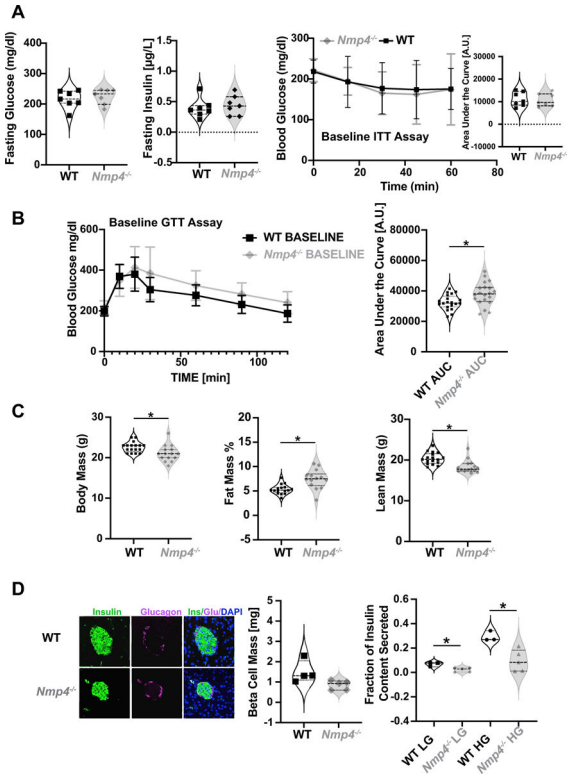

Figure 3: Nmp4$^{-/-}$ mice exhibit an intrinsic defect in β cell function and total body glucose homeostasis.

[A] *Nmp4*$^{-/-}$ and WT mice showed no differences in baseline glycemia, insulinemia, or insulin sensitivity. Statistical analyses were performed using a two-tailed t-test and significance was set at p≤ 0.05. Data represent average ± SD; n = 7 mice/group**. [B]** The *Nmp4*$^{-/-}$ mice showed a modest but significant impairment in glucose tolerance. GTT assay [first panel], *Nmp4*$^{-/-}$ and WT littermate controls, 8wks of age were fasted for 6 hours and given an I.P. injection of glucose at a dose of 1g/kg to assess glucose tolerance. AUC (area under curve, second panel) analysis, n=20/cohort, differences between means analyzed by a two-tailed, t-test, asterisk p<0.05. **[C]** EchoMRI shows that loss of *Nmp4*$^{-/-}$ alters baseline body composition. *Nmp4*$^{-/-}$ mice (8wks) exhibited a modest but significant lower body weight (first panel) and lean mass (third panel) but significant increase in % fat (second panel). Statistical analyses were performed using a two-tailed t-test and significance was set at p≤ 0.05. Data represent average ± SD; n = 15–17 mice/group **[D]** Pancreatic β-cell function is attenuated in the *Nmp4*$^{-/-}$ mice. Immunofluorescent staining of male (8wks) WT and *Nmp4*$^{-/-}$ pancreas sections showing expression of indicated proteins (first panel). WT mice show an average β-cell mass of 1.49 ± 0.55 mg (n=4 biological replicates; 12 total technical replicates]. *Nmp4*$^{-/-}$ mice show an average β-cell mass of 0.85 ± 0.23 mg (n=5 biological replicates; 15 total technical replicates), p=0.06 Statistical analysis was performed using a nested, mixed model ANOVA and significance was set at p≤ 0.05. In vitro GSIS assay (third panel) showing that *Nmp4*$^{-/-}$ islet cells have an attenuated insulin secretion compared to WT (n= 3 [WT], n=5 [*Nmp4*$^{-/-}$] biological replicates, average ± SD, asterisk = p<0.05 t-test. Abbreviations: GSIS, glucose-stimulated insulin secretion; HG, high glucose; LG, low glucose.

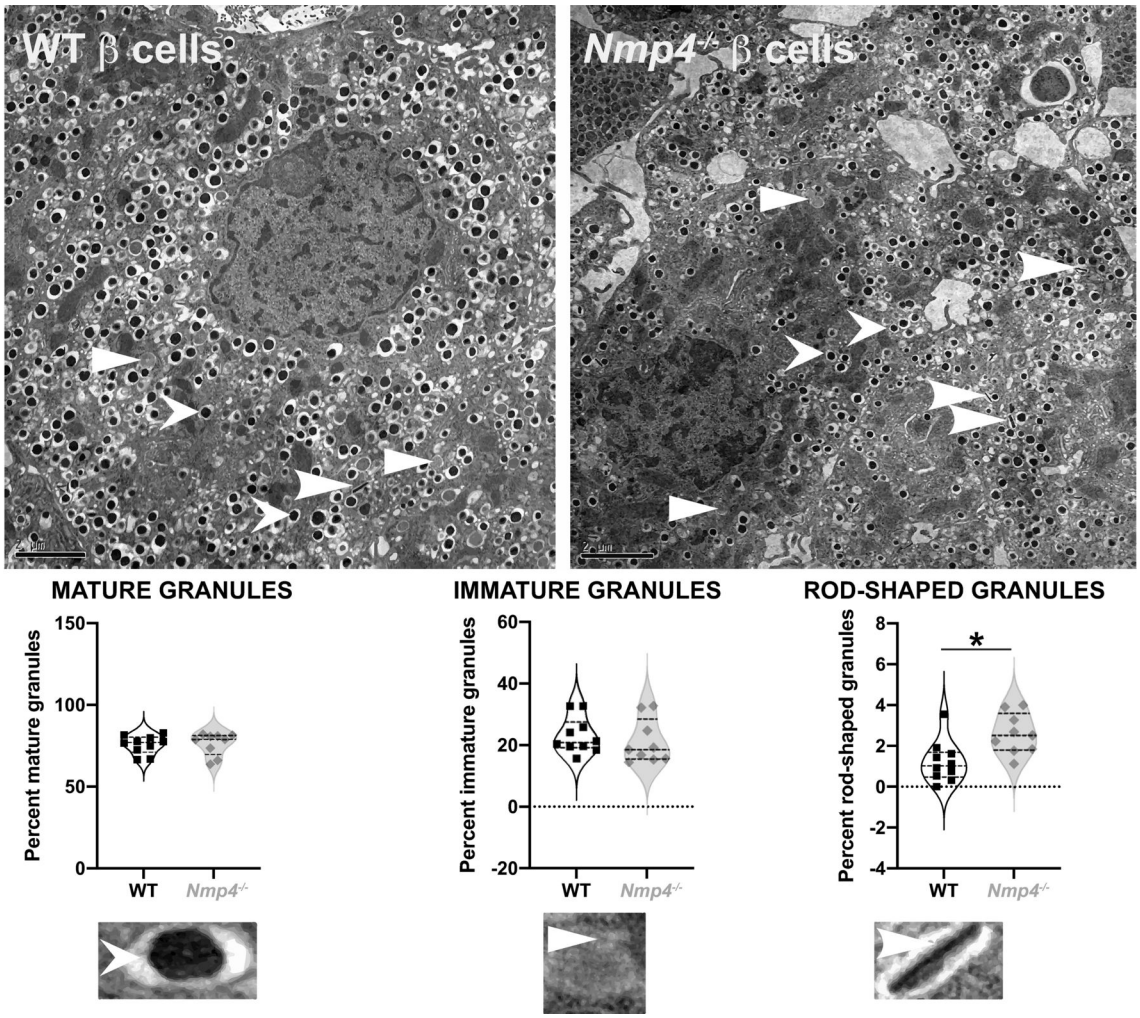

Figure 4:

Ultrastructure analyses of WT and *Nmp4*$^{-/-}$ islets. There are no differences in the percent of dense core mature insulin granules (dart/chevron symbol) or immature secretory granules (triangle symbol) between the genotypes. However, there is an increased number of rod-shaped granules (curved arrowhead) in the *Nmp4*$^{-/-}$ islets. Statistical analyses were performed using a non-parametric t-test and significance was set at $p \leq 0.05$. Data represent average ± SD (see Material and Methods for details).

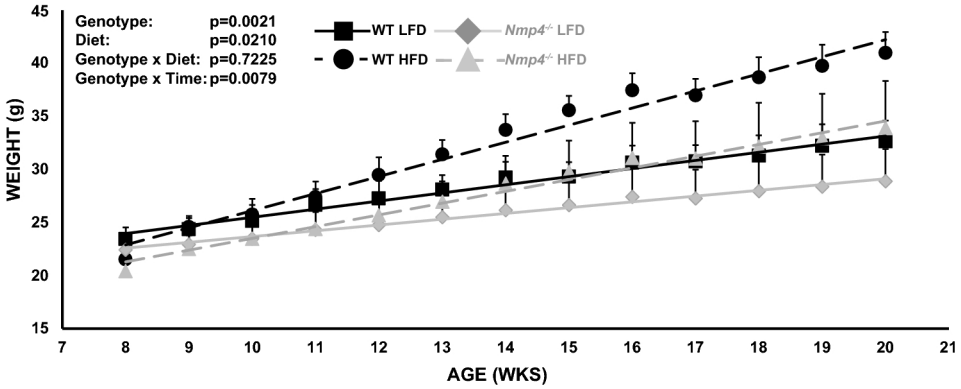

Figure 5: Nmp4$^{-/-}$ mice are less sensitive to HFD-induced weight gain (8wks-20wks of age).

Male WT and *Nmp4*$^{-/-}$ mice (8wks of age) were sorted randomly by weight into four treatment cohorts including (i) WT LFD; (ii) WT HFD; (iii) *Nmp4*$^{-/-}$ LFD; (iv) *Nmp4*$^{-/-}$ HFD. The mice were fed ad libitum either Teklad TD.88137 (adjusted calories diet 42% from fat) or the Teklad TD.05230 control diet. Treatment lasted 12wks (20wks of age). Statistical analysis reveals strong genotype (p=0.0021) and diet (p=0.0210) effects but no genotype x treatment interaction (p=0.7225). A slower rate of weight accrual is indicated for the *Nmp4*$^{-/-}$ mice by a significant genotype x time interaction (p=0.0079). A repeated-measures multivariate analysis of variance (RM MANOVA) was used to determine the listed p values (n= 10/cohort and 5–10 measurements/time point)

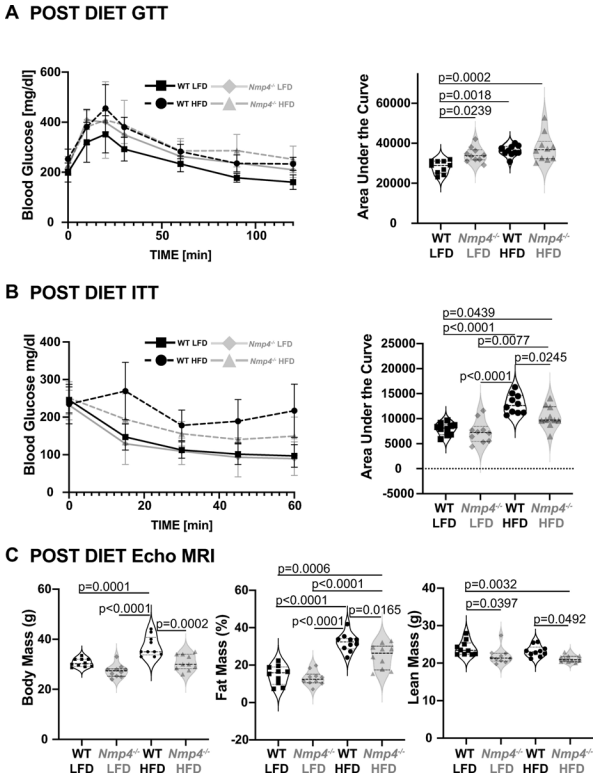

Figure 6: Nmp4$^{-/-}$ mice are less sensitive to HFD-induced changes in global glucose homeostasis

[A] Male WT mice exhibited a decrease in glucose tolerance on the HFD vs. LFD whereas the *Nmp4*$^{-/-}$ mice showed no change. GTT were performed after 12 weeks of HFD/LFD treatment in WT and *Nmp4*$^{-/-}$ mice; area under the curve (AUC) analysis is shown graphically. First panel, GTT assay, *Nmp4*$^{-/-}$ and WT littermate controls, 20wks of age were fasted for 6 hours and given an I.P. injection of glucose at a dose of 1g/kg to assess glucose tolerance. **[B]** Both WT and *Nmp4*$^{-/-}$ mice showed a decrease in insulin sensitivity on the HFD vs. LFD but the *Nmp4*$^{-/-}$ mice were significantly less affected by this challenge. **[C]** EchoMRI shows that *Nmp4*$^{-/-}$ mice were less sensitive to gains in body mass and %fat mass on the HFD compared to the WT mice. HFD did not alter lean mass in either genotype and *Nmp4*$^{-/-}$ mice exhibited lower lean mass than WT on both diets. All data are represented as average ± SD n=10/cohort. Statistical analyses: Two-way ANOVAs were performed using diet and genotype as main effects. The results of this analysis follow: GTT: Genotype p=0.0123, Treatment p=0.0003, GxT p=0.12; ITT: Genotype p=0.0132, Treatment p<0.0001, GxT p=0.11; BODY MASS: Genotype p<0.0001, Treatment p<0.0001, GxT p=0.11; % FAT MASS: Genotype p=0.0088, Treatment p<0.0001, GxT p=0.10; LEAN MASS: Genotype p=0.0004, Treatment p=0.16, GxT p=0.95. When a significant main effect was indicated, all pairwise post hoc comparisons were conducted to identify intergroup differences. Those comparisons yielding p values ≤ 0.05, are indicated in the panel.

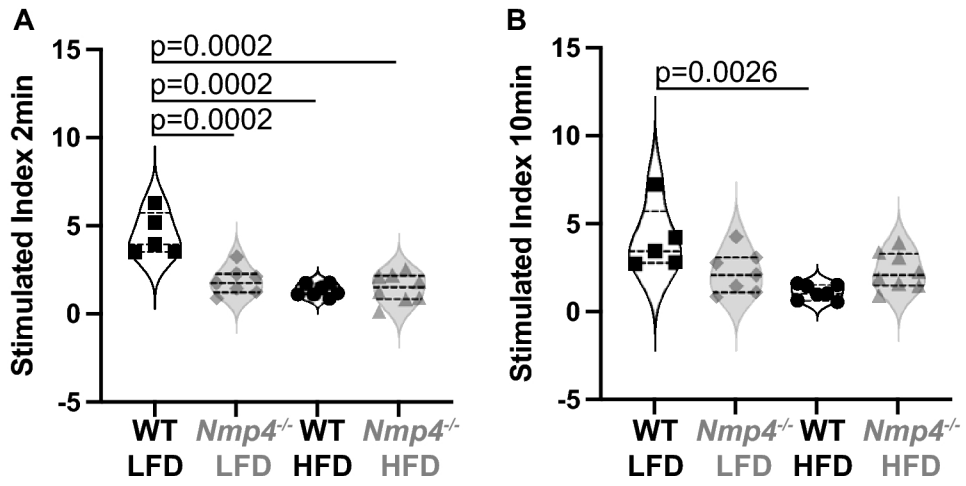

Figure 7: Nmp4$^{-/-}$ mice exhibit decreased insulin secretion.

ivGSIS were performed after 12wks of HFD/LFD treatment in WT and *Nmp4*$^{-/-}$ mice. The mice were fasted overnight and then injected intraperitoneally with 2g/kg body weight of glucose. Serum was obtained at time 0, 2, and 10 min following glucose injection. *Nmp4*$^{-/-}$ mice on LFD displayed significantly decreased circulating insulin compared to their WT LFD cohorts. Interestingly, HFD did not further exacerbate the attenuated glucose-induced insulin secretion in the *Nmp4*$^{-/-}$ mice but significantly lowered this response in the WT HFD group.

Two-way ANOVAs were performed using diet and genotype as main effects. The results of this analysis follow: Stimulated Index 2 minutes: Genotype p=0.0007, Treatment p<0.0001, GxT p=0.0002; Stimulated Index 10 minutes: Genotype p=0.5008, Treatment p=0.0041, GxT p=0.0026. When a significant main effect was indicated, all pairwise post hoc comparisons were conducted to identify intergroup differences. Those comparisons yielding p values ≤ 0.05, are indicated in the panel. Data represent average ± SD; n = 10 mice/group.

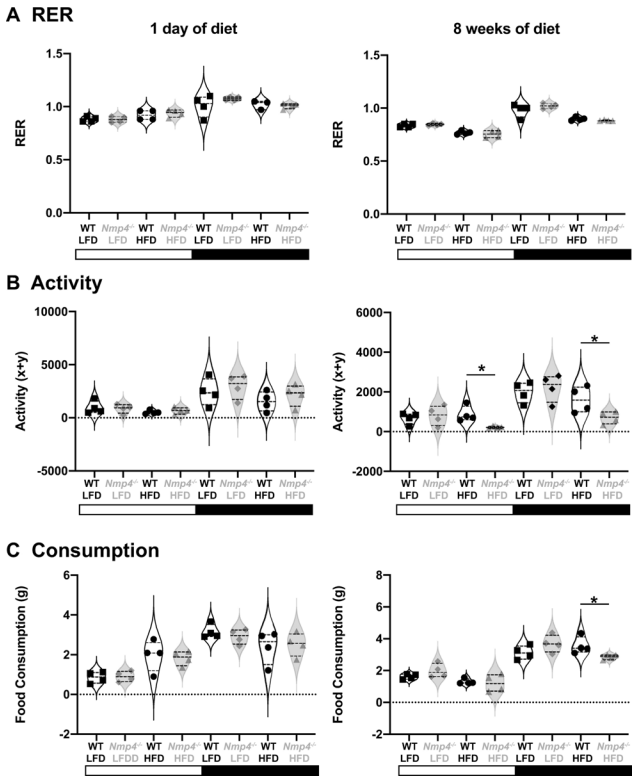

Figure 8: Nmp4$^{-/-}$ mice are more sensitive to HFD-induced changes in activity.

Metabolic cage studies were undertaken as described in Materials and Methods. **[A]** Loss of *Nmp4* did not alter the respiratory exchange ratio (RER). **[B]** There was no difference in mouse activity between the genotypes on the LFD but the *Nmp4*$^{-/-}$ HFD mice were less active and **[C]** consumed less food at night than WT HFD mice. All data are represented as average ± SD n=3–4/cohort. Differences between means analyzed by unpaired, two-tailed t-tests, asterisk $p<0.05$. The white and black bars represent Day and Night, respectively.

TABLE 1

HFD induced significant bone loss in both WT and *Nmp4*$^{-/-}$ mice.

PARAMETER	WT	*Nmp4* $^{-/-}$	p value Diet	p value Genotype	p value Interaction
Femur Trabecular Bone					
Tb N [mm^{-1}]	LFD = 3.86 ± 0.51 HFD = 3.25 ± 0.26	LFD = 3.72 ± 0.32 HFD = 3.20 ± 0.19	p<0.0001 LFD >HFD	p=0.40 WT = *Nmp4*$^{-/-}$	p=0.72
Tb. Sp [mm]	LFD = 0.164 ± 0.014 HFD = 0.178 ± 0.010	LFD = 0.164 ± 0.007 HFD = 0.174 ± 0.008	p = 0.0003 HFD >LFD	p=0.49 WT = *Nmp4*$^{-/-}$	p=0.57
Tb.TMD [mgHA/cm^3]	LFD = 0.761 ± 0.024 HFD = 0.749 ± 0.027	LFD = 0.754 ± 0.022 HFD = 0.728 ± 0.019	p = 0.01 LFD >HFD	p=0.07 WT = *Nmp4*$^{-/-}$	p=0.35
Tb Th [mm]	LFD = 0.0686 ± 0.0049 HFD = 0.0680 ± 0.0039	LFD = 0.0660 ± 0.0044 HFD = 0.0610 ± 0.0012	p =0.03 LFD > HFD	p=0.0004 WT > *Nmp4*$^{-/-}$	p=0.86
Femur Cortical Bone					
Femur length [mm]	LFD = 15.82 ± 0.34 HFD = 15.71 ± 0.23	LFD = 15.32 ± 0.25 HFD = 15.15 ± 021	p = 0.10 LFD = HFD	p<0.0001 WT> *Nmp4*$^{-/-}$	p=0.76
Marrow Area [mm^2]	LFD = 1.17 ± 0.09 HFD = 1.11 ± 0.16	LFD = 1.06 ± 0.12 HFD = 1.00 ± 0.07	p = 0.09 LFD = HFD	p=0. 0051 WT> *Nmp4*$^{-/-}$	p=0.92
Cortical Area [mm^2]	LFD = 1.10 ± 0.10 HFD = 0.99 ± 0.10	LFD = 1.02 ± 0.10 HFD = 0.88 ± 0.03	p = 0. 0002 LFD > HFD	p=0.0014 WT> *Nmp4*$^{-/-}$	p=0.58
Periosteal BS [mm]	LFD = 6.15 ± 0.20 HFD = 5.96 ± 0.33	LFD = 5.92 ± 0.28 HFD = 5.64 ± 0.13	p = 0.0049 LFD >HFD	p= 0.0012 WT> *Nmp4*$^{-/-}$	p=0.57
Endocortical BS [mm]	LFD = 4.85 ± 0.20 HFD = 4.72 ± 0.36	LFD = 4.67 ± 0.27 HFD = 4.42 ± 0.17	p = 0.02 LFD >HFD	p= 0.0051 WT> *Nmp4*$^{-/-}$	p=0.47
I_{MAX} [mm^4]	LFD = 0.422 ± 0.066 HFD = 0.372 ± 0.092	LFD = 0.357 ± 0.077 HFD = 0.276 ± 0.030	p = 0.0054 LFD >HFD	p= 0.0009 WT> *Nmp4*$^{-/-}$	p=0.49
I_{MIN} [mm^4]	LFD = 0.213 ± 0.040 HFD = 0.176 ± 0.035	LFD = 0.182 ± 0.041 HFD = 0.147 ± 0.010	p = 0.0019 LFD >HFD	p= 0.0089 WT> *Nmp4*$^{-/-}$	p=0.95

Femoral trabecular and cortical architecture from WT and *Nmp4*$^{-/-}$ mice placed on LFD or HFD from 8wks to 20wks of age. Imin and Imax are the minimum and maximum moment of inertia at the cross-section. Statistical analyses were performed using two-way ANOVA tests setting genotype and diet as the independent variables. Statistical significance was set at p≤ 0.05. Data represent average ± SD; n = 10 mice/group.

TABLE 2

HFD altered some femoral bone mechanical properties in both WT and *Nmp4*$^{-/-}$ mice placed on LFD or HFD from 8wks to 20wks of age.

PARAMETER	WT	*Nmp4* $^{-/-}$	p value Diet	p value Genotype	p value Interaction
Yield Force [N]	LFD = 12.21 ± 1.64 HFD = 11.69 ± 1.64	LFD = 11.47 ± 1.56 HFD = 10.52 ± 1.77	p=0.19 LFD = HFD	p=0.08 WT = *Nmp4*$^{-/-}$	p=0.69
Ultimate Force [N]	LFD = 20.36 ± 2.69 HFD = 17.59 ± 2.14	LFD = 18.82 ± 2.93 HFD = 15.61 ± 1.35	p=0.0003 LFD >HFD	p=0.02 WT > *Nmp4*$^{-/-}$	p=0.78
Displacement to yield [μm]	LFD = 121.38 ± 12.92 HFD = 139.41 ± 23.40	LFD = 122.23 ± 26.92 HFD = 131.01 ± 16.11	p = 0.05 HFD >LFD	p=0.56 WT = *Nmp4*$^{-/-}$	p=0.48
Post-yield Displacement (μm)	LFD = 404 ± 128.62 HFD = 326.3 ± 178.20	LFD = 341.33 ± 154.53 HFD = 395 ± 173.65	p=.0.82 LFD = HFD	p=0.95 WT = *Nmp4*$^{-/-}$	p=0.21
Total Displacement [μm]	LFD = 525.38 ± 135.16 HFD = 465.71 ± 191.31	LFD = 463.56 ± 142.49 HFD = 526.01 ± 175.31	p =0.98 LFD = HFD	p=0.99 WT = *Nmp4*$^{-/-}$	p=0.25
Stiffness (N/mm)	LFD = 117.47 ± 17.34 HFD = 97.57 ± 11.26	LFD = 112.91 ± 19.96 HFD = 93.21 ± 4.31	p = 0.0001 LFD > HFD	p=0.34 WT = *Nmp4*$^{-/-}$	p=0.98
Work to Yield (mJ)	LFD = 0.835 ± 0.158 HFD = 0.921 ± 0.261	LFD = 0.803 ± 0.243 HFD = 0.790 ± 0.221	p = 0.61 LFD = HFD	p=0.26 WT = *Nmp4*$^{-/-}$	p=0.49
Post-yield Work (mJ)	LFD = 7.10 ± 2.35 HFD = 5.00 ± 2.79	LFD = 5.69 ± 3.33 HFD = 5.32 ± 2.34	p = 0.16 LFD = HFD	p=0.54 WT = *Nmp4*$^{-/-}$	p=0.33
Total Work (mJ)	LFD = 7.94 ± 2.42 HFD = 5.92 ± 2.95	LFD = 6.50 ± 3.21 HFD = 6.11 ± 2.39	p= 0.18 LFD = HFD	p= 0.48 WT = *Nmp4*$^{-/-}$	p=0.36
Yield Stress (MPa)	LFD = 81.83 ± 8.79 HFD = 88.98 ± 10.05	LFD = 88.64 ± 18.34 HFD = 95.31 ± 19.11	p = 0.15 LFD = HFD	p= 0.17 WT = *Nmp4*$^{-/-}$	p=0.96
Ultimate Stress (MPa)	LFD = 136.20 ± 10.08 HFD = 133.69 ± 9.36	LFD = 142.58 ± 11.40 HFD = 140.54 ± 11.09	p = 0.45 LFD = HFD	p= 0.06 *Nmp4*$^{-/-}$> WT	p=0.94
Strain to Yield [μstrain]	LFD = 14888 ± 1822 HFD = 15951 ± 3180	LFD = 14722 ± 3443 HFD = 14718 ± 1913	p = 0.54 LFD = HFD	p= 0.42 WT = *Nmp4*$^{-/-}$	p=0.54
Total Strain [μstrain]	LFD =64283 ± 16583 HFD =53480 ± 23188	LFD =56384 ± 19637 HFD=59104 ± 19763	p = 0.54 LFD = HFD	p= 0.85 WT = *Nmp4*$^{-/-}$	p=0.29
Modulus [GPa]	LFD = 6.45 ± 0.92 HFD = 6.60 ± 1.11	LFD = 7.13 ± 1.07 HFD= 7.50 ± 0.63	p = 0.41 LFD = HFD	p= 0.01 *Nmp4*$^{-/-}$> WT	p=0.73
Resilience [MPa]	LFD = 0.69 ± 0.13 HFD = 0.80 ± 0.20	LFD = 0.76 ± 0.29 HFD = 0.81 ± 0.25	p = 0.27 LFD = HFD	p= 0.58 *Nmp4*$^{-/-}$= WT	p=0.67
Toughness [MPa]	LFD = 6.56 ± 1.98 HFD = 5.04 ± 2.27	LFD = 5.81 ± 2.24 HFD = 6.21 ± 2.49	p = 0.44 LFD = HFD	p= 0.77 *Nmp4*$^{-/-}$= WT	p=0.19

Mechanical and material properties derived from femoral 3-point bending analysis. Statistical analyses were performed using two-way ANOVA tests setting genotype and diet as the independent variables. Statistical significance was set at p≤ 0.05. Data represent average ± SD; n = 10 mice/group.